Ribbon Formation in Twist-Nematic Elastomers

L. Teresi* **and V. Varano**

LaMS – Modelling & Simultation Lab, Università Roma Tre, Italy

***Corresponding author: Via C. Segre 4/6, 00146, Roma, Italy, email: teresi@uniroma3.it**

Abstract: Nematic Elastomers (NEs) possess very interesting properties stemming from the interaction between liquid crystal order and rubber elasticity. For such materials, thermally-induced phase transition from the isotropic to the nematic phase may induce very large distortions, which in turn can affect the overall configuration of a macroscopic specimen. The behavior of NEs can be well modeled within the theory of finite elasticity with distortions; here, we test a theoretical model against fancy shapes formation; in particular, we deal with the many different shapes that a thin, slender bar, made of NE, may assume as a consequence of its chiral symmetry during solvent evaporation and subsequent heating. Our goal has been to replicate with numerical experiments the phenomena of shape formation in chiral NEs, and our results constitute a noteworthy assessment of the physical model underlying the numerical solutions.

Keywords: Shape formation, Liquid crystal elastomer, nematic- isotropic phase transition, swelling.

1. Introduction

Nematic Elastomers (NEs) possess very interesting properties stemming from the interaction between liquid crystal order and rubber elasticity [1]. Such materials exhibit a direct coupling between the mesogen alignment and their overall conformation; as a result, the nematic effect on the macroscopic properties can be of the essence in determining the actual shape of a given specimen, especially for monodomain NEs, characterized by a regular nematic alignement.

A particular class of NEs features two sorts of large, anisotropic, transformations: the first one, thermally induced, is due to an isotropic-nematic phase transition; the second one is a deswelling that manifests if solvent evaporates at the nematic state. Both phenomena can produce large changes of configuration in a macroscopic specimen, with a noticeable distinction: during solvent evaporation the nematic order is strongly coupled with volume as well as shape, and deswelling induces permanent, anisotropic shape changes; conversely, the thermal effects are reversible: cooling below a transition temperature T_{NI} increases the nematic order, thus driving a spontaneous elongation along the nematic direction, whereas heating towards T_{NI} induces a reverse deformation.

The behavior of NEs can be well modeled within the theory of finite elasticity with distortions; here, the same model used in [3] is tested against more fancy shapes formation; in particular, we have been prompted by the new interesting results published in [4], and we deal with the many different shapes that a thin, slender bar, may assume as a consequence of its chiral symmetry during solvent evaporation and heating. Our goal has been to replicate with numerical experiments the phenomena of shape formation in twist-nematic elastomers (TNEs), and our results constitute a noteworthy assessment of the physical model underlying the numerical solutions. A detailed description about preparation of TNEs, and experimental results is given in [4].

2. The physical model

We model the NEs in the framework of nonlinear elasticity with large distortions [2]. We consider a material whose state is described, apart from a displacement field $\mathbf{u}$, by the pair (ϑ, v): the reduced temperature $\vartheta = T/T_{NI}$ is the ratio between the actual temperature T, and the transition temperature T_{NI}; the second one $v = V/V_o$ measures the ratio between the actual volume V and the initial one V_o. We represent the nematic orientation with the nematic tensor field $\mathbf{N} := \mathbf{n} \otimes \mathbf{n}$, with $\mathbf{n}$, the director, a unit vector field ($|\mathbf{n}| = 1$).

A key feature of the *elastomeric distortions* we deal with is that they are sensible to both solvent evaporation and temperature, and both can

be described by uniaxial stretches aligned with the nematic orientation $\mathbf{N}$:

$$\begin{aligned}\mathbf{U}_v(v) &= \alpha_\parallel(v)\,\mathbf{N} + \alpha_\perp(v)\,(\mathbf{I}-\mathbf{N})\,,\\ \mathbf{U}_\vartheta(\vartheta) &= \lambda_\parallel(\vartheta)\,\mathbf{N} + \lambda_\perp(\vartheta)\,(\mathbf{I}-\mathbf{N})\,.\end{aligned} \tag{1}$$

where $\mathbf{I}$ is the identity. The scalars $\alpha_\parallel(v)$ and $\alpha_\perp(v)$ represent the magnitude of the deswelling-induced stretches, at constant temperature, along $\mathbf{n}$, and on the plane orthogonal to $\mathbf{n}$, respectively; the stretches $\lambda_\parallel(\vartheta)$, $\lambda_\perp(\vartheta)$ are instead temperature dependent. It is worth noting that the nematic-isotropic transition is volume preserving, while deswelling is not:

$$\lambda\|(\vartheta)\,\lambda_\perp^2(\vartheta) = 1\,, \quad \alpha\|(v)\,\alpha_\perp^2(v) = v\,. \tag{2}$$

The preparation state $(\vartheta, v) = (\vartheta_o, 1)$, with $\vartheta_o = T_o/T_{NI}$ is assumed as reference; thus, we define the resultant distortion $\mathbf{U}_o(\vartheta, v) = \mathbf{U}_\vartheta(\vartheta)\,\mathbf{U}_\vartheta^{-1}(\vartheta_o)\,\mathbf{U}_v(v)$: it follows from (1)

$$\mathbf{U}_o(\vartheta, v) = \frac{\lambda_\parallel(\vartheta)\,\alpha_\parallel(v)}{\lambda_\parallel(\vartheta_o)}\,\mathbf{N} + \frac{\lambda_\perp(\vartheta)\,\alpha_\perp(v)}{\lambda_\perp(\vartheta_o)}\,(\mathbf{I}-\mathbf{N})\,. \tag{3}$$

Relation (3) prompts the introduction of the *resultant stretches*:

$$\Lambda_\parallel(\vartheta, v) = \frac{\lambda_\parallel(\vartheta)\,\alpha_\parallel(v)}{\lambda_\parallel(\vartheta_o)}\,, \quad \Lambda_\perp(\vartheta, v) = \frac{\lambda_\perp(\vartheta)\,\alpha_\perp(v)}{\lambda_\perp|(\vartheta_o)}\,, \tag{4}$$

which account for both solvent evaporation and temperature change. In actual experiments it is possible to measure the deswelling distortions $\alpha_\parallel^d = \alpha_\parallel(v_d)$, $\alpha_\perp^d = \alpha_\perp(v_d)$ at the dry state v_d; also, by measuring the temperature dependent stretches, a fitting expression for $\lambda_\parallel(\vartheta)$ can be determined:

$$\lambda_\parallel(\vartheta) = \begin{cases} \left[1+\beta(1-\vartheta)^a\right]^{1/2}, & \vartheta < 1;\\ 1\,, & \vartheta \geq 1\,. \end{cases} \tag{5}$$

Within the theory of elasticity, distortions describe the change of ground states, that is, states at zero elastic energy. Thus, given a displacement field $\mathbf{u}$ with respect to the preparation state, its gradient $\mathbf{F} = \mathbf{I} + \nabla\mathbf{u}$ describes the actual deformation of volume elements; the difference between actual deformation and distortion is measured by the elastic deformation $\mathbf{F}_e = \mathbf{F}\,\mathbf{U}_o^{-1}$, and the elastic energy has to be a function of the *elastic strain* $\mathbf{C}_e$, defined as

$$\mathbf{C}_e = \mathbf{F}_e^\top\,\mathbf{F}_e = \mathbf{U}_o^{-\top}\mathbf{C}\,\mathbf{U}_o^{-1}\,, \quad \text{with} \quad \mathbf{C} = \mathbf{F}^\top\,\mathbf{F}\,. \tag{6}$$

We consider here a Neo-Hookean energy, the simplest non-linear elastic energy, given by

$$\begin{aligned}&\phi(\mathbf{C}_e) = \tfrac{1}{2}\,\mu\,(\mathbf{C}^e\cdot\mathbf{I}-3) = \tfrac{1}{2}\,\mu\,(\mathbf{C}\cdot\mathbf{C}_o^{-1}-3)\,,\\ &\det(\mathbf{C}_o) = v^2,\end{aligned} \tag{7}$$

with μ the shear modulus, and $\mathbf{C}_o$ the distortional strain induced by $\mathbf{U}_o$:

$$\mathbf{C}_o(\vartheta, v) = \mathbf{U}_o^\top(\vartheta, v)\,\mathbf{U}_o(\vartheta, v)\,. \tag{8}$$

It can easily be verified that the preparation state (nematic-swollen) realizes the reference configuration:

$$(\vartheta, v) = (\vartheta_o, 1) \;\Rightarrow\; \mathbf{U}_o = \mathbf{I} \;\Rightarrow\; \mathbf{C}_o = \mathbf{I} \;\Rightarrow\; \mathbf{C} = \mathbf{I}\,;$$

moreover, another global stress-free configuration exists, the one corresponding to the flat temperature ϑ_f

$$(\vartheta_f, v_d) \;\Rightarrow\; \mathbf{C}_o = v_d^{2/3}\mathbf{I} \;\Rightarrow\; \mathbf{C} = v_d^{3/2}\mathbf{I}\,.$$

3. Twist-Nematic Elastomers

The model presented in the previous section is used to simulate the behavior of slender bars made of NEs, fabricated with a chiral arrangement of liquid crystal mesogens. We consider as reference configuration a slender bar $\mathcal{B}$ of sides $L\times W\times H$ representing the specimen at the preparation state, $(\vartheta, v) = (\vartheta_o, 1)$, that is, nematic and swollen. We denote with $\{o; x, y, z\}$ a Cartesian frame having its origin o at the center of $\mathcal{B}$, and the three axes aligned with L, W, and H, respectively; finally, $\mathbf{e}_i$, $i = 1, 2, 3$ are three unit vectors parallel to the coordinate axes. We assume the nematic tensor $\mathbf{N}$ to lie in the horizontal plane x, y, and having a linear twist along z, with a twist angle span $\alpha_s = \pi/2$. Denoted with α the angle between the director $\mathbf{n}$ and the long axis of the bar, we consider two director arrangements:

$$\alpha(z) = -\frac{\alpha_s}{H}\,z\,, \quad \alpha(z) = -\frac{\alpha_s}{H}\,z + \frac{\pi}{2}\,, \tag{9}$$

dubbed L- and S-geometry, respectively, see Fig.1.

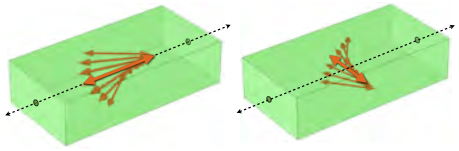

Figure 1: Left, L-geometry: the nematic axis at mid plane (thick arrow) is aligned with the long axis of the bar (thin arrow, dashed). Right, S-geometry: the nematic axis at mid plane is orthogonal to the long axis of the bar.

4. Model implementation

Aimed at investigating the phenomena of shape formation, we perform a series of numerical experiments on TNE bars $\mathcal{B}$, having different cross-sectional aspect ratios W/H, ranging from ~ 6 (narrow bar) to ~ 22 (wide bar), and for both the nematic geometries (L- and S-geometry). Our specimens are unloaded, and clamped at the face $x = -L/2$ in order to eliminate rigid motions.

In particular, for each specimen, we first simulate deswelling, by solving a sequence of N elastic problems corresponding to (ϑ_o, v_i), where v_i is a monotone decreasing sequence, with $v_1 = 1$, $v_N = v_d < 1$. The final solution we obtain corresponds to the dry-nematic state, and it is used as initial condition to simulate the heating process; then, we solve another sequence of N elastic problems for (ϑ_i, v_d), where ϑ_i is a monotone increasing sequence, with $\vartheta_1 = \vartheta_o$, $\vartheta_N = 1$.

We implement the balance equations of non-linear elasticity in weak form, using the volumetric-deviatoric decomposition of the deformation measures, and adopting a mixed method. Thus, we have as independent variables the displacement vector $\mathbf{u}$, and the pressure p; given $\mathbf{F} = \mathbf{I} + \nabla\mathbf{u}$, we consider the following relaxed strain energy density: $\phi_r = \phi_s + \phi_v$, with

$$\begin{aligned}
&\phi_s = \tfrac{1}{2}\,\mu\,(\mathbf{C}_s \cdot \mathbf{C}_o^{-1} - 3) && \text{isochoric energy;}\\
&\phi_v = \tfrac{k}{2}\,(J - v)^2 && \text{volumetric energy;}\\
&\mathbf{C}_s = (v/J)^{2/3}\,\mathbf{C}\,, && \text{unimodular part of } \mathbf{C};\\
&p = -k\,(J - v)\,, && \text{pressure;}\\
&J = \det(\mathbf{F})\,, && \text{volume change;}
\end{aligned} \tag{10}$$

and k the bulk modulus. The reference stress $\mathbf{S}$ and the actual stress $\mathbf{T}$ are then given by

$$\begin{aligned}
&\mathbf{S} = 2\,\mathbf{F}^e\,\mathbf{S}_{sc}\,\bar{\mathbf{F}}_o^* - p\,\mathbf{F}^*,\\
&\mathbf{T} = \mathbf{S}\,(\mathbf{F}^*)^{-1}
\end{aligned} \tag{11}$$

with $\mathbf{A}^* = \det(\mathbf{A})\,\mathbf{A}^{-\top}$ denoting the cofactor of $\mathbf{A}$, and

$$\mathbf{S}_{sc} = \frac{\partial \phi_s}{\partial \mathbf{C}^e} = \frac{1}{2}\,\mu\,J_e^{-2/3}\left(\mathbf{I} - \frac{1}{3}\,\mathrm{tr}(\mathbf{C}^e)\,(\mathbf{C}^e)^{-1}\right), \tag{12}$$

where $J_e = \det(\mathbf{F}^e) = J/v$. It follows

$$\begin{aligned}
&\mathbf{S} = \mu\,v\,\mathbf{F}\,\mathbf{C}_o^{-1} - p\mathbf{F}^*\,;\\
&\mathbf{T} = \mu\,\frac{1}{J_e}\,\mathbf{F}_e\,\mathbf{F}_e^{\top} - p\,\mathbf{I}\,.
\end{aligned} \tag{13}$$

From (8), (13) it follows that the reference stress is a function of the independent variables $\mathbf{u}$ and p, and of the state variables (ϑ, v):

$$\mathbf{S} = \mathbf{S}(\mathbf{u}, p; \vartheta, v)\,. \tag{14}$$

Thus, we can solve our problem for $\mathbf{u}$ and p, using the pair (ϑ, v) as parameters; in particular, using the parametric solver, we first simulate deswelling, by solving a sequence of N elastic problems corresponding to (ϑ_n, v_i), with $v_1 = 1$, $v_N = v_d < 1$. The final solution we obtain corresponds to the dry-nematic state, and it is used as initial data to simulate the heating process; thus, we solve another sequence of N elastic problems for (ϑ_i, v_d), with $\vartheta_1 = \vartheta_n$, $\vartheta_N = 1$.

5. Results

Our main findings are listed here:

- The deformed configuration can be well described by its mid surface.
- There exist two different deformation modes: the helicoid (Mode I) and the spiral ribbon (Mode II).
- The shape transition from helicoid to spiral ribbon is ruled by $\|\Lambda_{\|} - \Lambda_{\perp}\|$.
- The handedness of the modes is ruled by the sign of $\Lambda_{\|}^2 - \Lambda_{\perp}^2$.

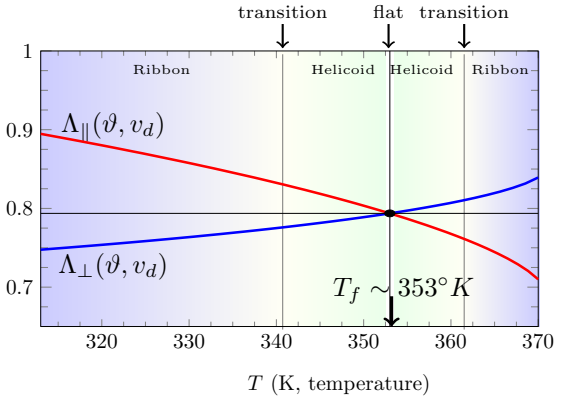

Figure 2: Evolution of resultant stretches $\Lambda_{\parallel}$ and $\Lambda_{\perp}$ during heating at constant volume v_d (solid lines). The shape transitions are for a TNE bar with $W/H \sim 15$.

Fig. 2 shows shape transitions for a typical TNE bar with $W/H \sim 15$. The range of temperature centered at T_f corresponding to helicoidal shapes changes with the ratio W/H; for small ratios, it becomes larger, and eventually the ribbon phase is never observed; conversely, for larger ratios it gets smaller, and helicoidal shapes can be realized only at temperature very close to T_f.

We analyze the geometric properties of the shapes we obtain using some basic notions of 2D differential geometry; the fundamental forms (FFs) relative to such shapes can be evaluated as follows from the results of our 3D numerical simulations: define the vector fields:

$$\mathbf{a}_i = (\mathbf{F}|_{z=0})\,\mathbf{e}_i\,, \quad \mathbf{n} = \frac{\mathbf{a}_1 \times \mathbf{a}_2}{|\mathbf{a}_1 \times \mathbf{a}_2|}\,, \tag{15}$$

then, compute the FFs

$$a_{ij} = \mathbf{a}_i \cdot \mathbf{a}_j \quad b_{ij} = \mathbf{n}_{,i} \cdot \mathbf{a}_j\,, \tag{16}$$

where $\mathbf{n}_{,i}$ denotes derivative of $\mathbf{n}$ with respect to the i-th coordinate. Global geometrical properties can then be evaluated from the FFs; among them, we list helicoid twist pitch, ribbon diameter, ribbon helical pitch and the handedness of the torsion.

Fig. 3 shows the value of b_{11}, the longitudinal curvature of the axis of the bar, versus the reduced temperature $\vartheta = T/T_{NI}$, for eight different bars having the same height, $H_f = 35\,\mu m$, and the same length ($L_f = 7000\,\mu m$), whose widths range from $W_f = 200\,\mu m$ to $W_f = 900\,\mu m$ (subscript "f" denotes that these values are referred to the flat state); the departure from the straight line denotes the onset of shape transition from helicoid to spiral ribbon. For the L-geometry, the plots relative to the first three cases are superimposed, and only the red line is visible: in the whole range of temperature change, such bars realize only helicoidal shapes; for the L-geometry, the plots relative to the first two cases are superimposed. The phenomenon of shape transition can

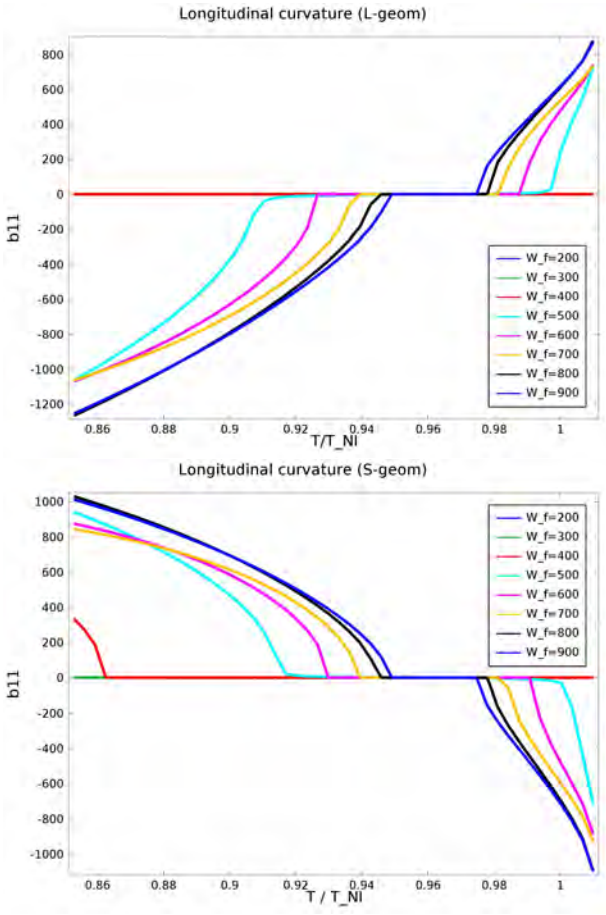

Figure 3: Longitudinal Curvature VS Reduced Temperature (L-geometry, top; S-geometry, bottom) for bar with same height but different width W_f; the departure from the straight line denotes the onset of shape transition.

be appreciated through Fig. 4: the plot at the center shows the evolution of resultant stretches $\Lambda_{\parallel}(\vartheta, v)$ and $\Lambda_{\perp}(\vartheta, v)$ during deswelling at constant temperature ϑ_o (dashed lines) and heating

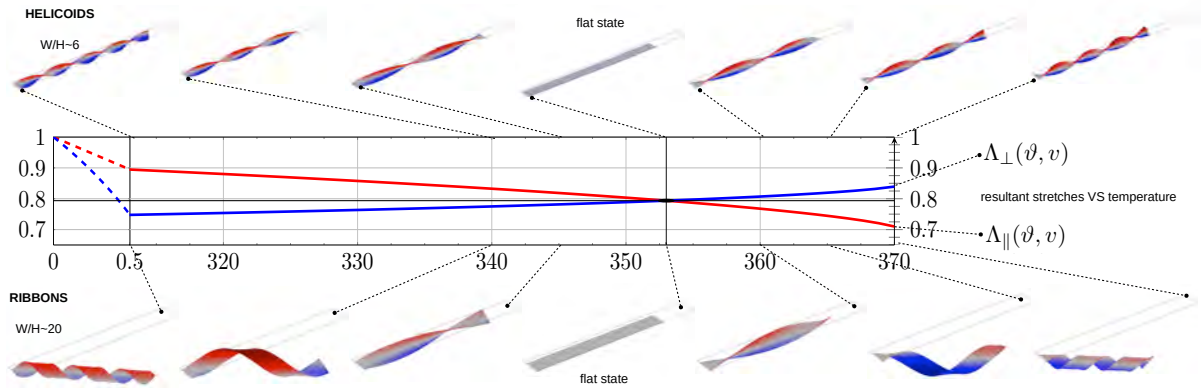

Figure 4: Evolution of resultant stretches $\Lambda_\parallel(\vartheta, v)$ and $\Lambda_\perp(\vartheta, v)$ during deswelling at constant temperature ϑ_o (dashed lines) and heating at constant volume v_d (solid lines). Cartoon at top and bottom shows the shape evolution of two slender bars with different cross-section aspect ratio.

at constant volume v_d (solid lines); thumbnails at top and bottom show the shape evolution of two slender bars having cross-section with different aspect ratio. For deswelling, the dashed lines represents just a possible path; for heating, the two lines are a straightforward consequence of (4, 5). Fig. (5) shows the shape change due to heating (increasing temperature from left to right) for a wide bar having an L-geometry and $W/H \sim 15$.

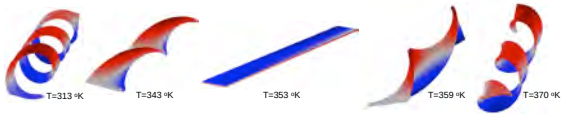

Figure 5: L-geometry, wide bar, increasing temperature from left to right. The specimen has a ribbon-like shape at low temperature; then it is a helicoid near the flat temperature, and becomes again a ribbon, with a different handedness, near the transition temperature.

$T_o = 313$ K	preparation temperature
$T_{NI} = 367$ K	transition temperature
$v_d = 0.5$	dry volume / initial volume
$\alpha^d_\parallel = 0.907$	dry parallel stretch
$\alpha^d_\perp = 0.743$	dry orthogonal stretch
$a = 2/3$, $\beta = 4.94$	fitting parameter for $\lambda_\parallel(\vartheta)$

Table 1: Numerical values used in numerical experiments

6. Conclusions

We are able to replicate the experimental findings in [4], thus having a robust assessment of the physical model underling the numerical solutions.

Acknowledgements The present work is supported by MIUR (the Italian Ministry of University and Research) through the Project PRIN2009 "Mathematics and Mechanics of Biological Assemblies and Soft Tissues".

References

[1] K. Urayama, Selected Issues in Liquid Crystal Elastomers and Gels. *Macromolecules* 40, 2277–2288 (2007).

[2] A. DeSimone, L. Teresi, Elastic energies for nematic elastomers. *Eur. Phys. J. E* 29, 191–204 (2009)

[3] Y. Sawa, K. Urayama, T. Takigawa, A. DeSimone, L. Teresi, Thermally Driven Giant Bending of Liquid Crystal Elastomer Films with Hybrid Alignment. *Macromolecules* 43, 4362–4369 (2010).

[4] Y. Sawa, F. Ye, K. Urayama, T. Takigawa, V. Gimenez-Pinto, R.L.B. Selinger, and J. V. Selinger, Shape selection of twist-nematic-elastomer ribbons. *PNAS*, 108/16, 6364–6368 (2011).